Available online at www.sciencedirect.com
ScienceDirect
Control Engineering Practice 16 (2008) 1081–1091
CONTROL ENGINEERING PRACTICE
www.elsevier.com/locate/conengprac

# Motion planning for experimental airpath control of a diesel homogeneous charge-compression ignition engine

Jonathan Chauvin[a,*], Gilles Corde[a], Nicolas Petit[b], Pierre Rouchon[b]

[a]Institut Français du Pétrole, 1 et 4 Avenue de Bois Préau, 92852 Rueil-Malmaison, France
[b]Centre Automatique et Systèmes, École des Mines de Paris, 60, bd St Michel, 75272 Paris, France

Received 18 January 2007; accepted 12 December 2007
Available online 1 February 2008

**Abstract**

A strategy based on motion planning is proposed for airpath control of turbocharged diesel engines equipped with exhaust gas recirculation. The objective is to manage the air and burned gas masses in the cylinder. The model considered uses simple balance equations for the intake manifold. The fully actuated dynamics are easily inverted, yielding straightforward open-loop control laws. This approach is complemented by experimentally derived look-up tables to apply driver requests into the problem of designing transitions between operating points. Experimental tests are reported for a four-cylinder homogeneous charge-compression ignition engine. Conclusions stress the possibility of taking into account the non-minimum phase effects of this system by a control law that is simple, yet efficient in practice.


*Keywords:* Engine control; Trajectory planning; Diesel engines; Non-minimum phase systems; Multivariable control

## 1. Introduction

### 1.1. Motivation

Performance and environmental requirements for diesel engines have steadily increased over the last 30 years, which in turn have prompted an increase in the sophistication of control strategies. Advances in combustion strategies over this period have been one of the keys in meeting such demands. Recently, the highly premixed combustion (HPC) mode—including homogeneous charge-compression ignition (HCCI)—has emerged as an efficient technology with low pollution. HCCI engines use a premixed charge of fuel and air and require the use of high exhaust gas recirculation (EGR) rates (typically more than 45% of the total gas flow).[1] Because the intake charge is diluted and premixed, the peak in-cylinder temperatures are significantly lower, resulting in the formation of very little $NO_x$ compared to conventional SI and CI internal combustion engines. However, this improvement in efficiency is at the expense of less stable combustion. Fig. 1 presents the cylinder pressures obtained for EGR valve variation at the engine testbed. A significant impact on the combustion process and the engine response in terms of $NO_x$ emission and noise production is evident, as presented in Fig. 2. Indeed, compared to the reference composition in the cylinder, an offset of +5% in burned gas may cause misfires, and an offset of −5% may increase the noise by +8 dB and lead to higher pollutant emissions. Close control of the masses of air and burned gas in the intake manifold is thus needed for correct HCCI combustion, which is the problem addressed in this paper.

### 1.2. Control problem

The ultimate goal of studies conducted in the Engine Control Department at Institut Français du Pétrole is real-time control of combustion. The approach is currently limited to managing the air and burned gas masses in the cylinder ($M_{asp,air}$ and $M_{asp,bg}$), but the plan is to consider

*Corresponding author. Tel.: +33 1 47527417; fax: +33 1 47527012.
*E-mail address:* jonathan.chauvin@ifp.fr (J. Chauvin).

[1]In the present case, as represented in Fig. 3, only a short-route EGR system is used, i.e. the exhaust gases are taken before the turbine to the intake manifold.

0967-0661/$ - see front matter © 2007 Elsevier Ltd. All rights reserved.
doi:10.1016/j.conengprac.2007.12.001

shorter time scales in the near future. Controlling the airpath dynamics is not an easy task. Fig. 3 shows a schematic diagram of the airpath of an EGR-equipped turbocharged diesel engine. The nomenclature is listed in Table 1. From a dynamical systems point of view, the airpath system of a turbocharged diesel engine features coupled dynamics (Kao & Moskwa, 1995; Kolmanovsky, Stefanopoulou, Moraal, & van Nieuwstadt, 1997; van Nieuwstadt et al., 1998). The main components of a diesel engine airpath are the cylinders, the intake manifold, the turbocharger and the EGR loop, as shown in Fig. 3. The turbocharger is used to feed the intake manifold with fresh air and the EGR loop carries exhaust gas. The gases are then mixed in the intake manifold, which in turn feeds the engine. At the exhaust, gases are directed to both the EGR loop and the turbine of the turbocharger to provide energy. One of the most important coupling points is that the EGR acts as a discharge valve for the turbocharger.

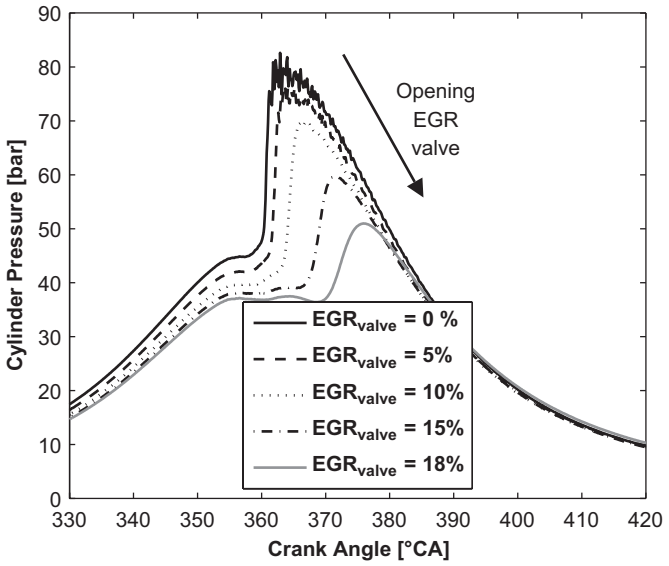


Fig. 1. Experimental variation of the EGR valve under fixed operating conditions (5 bar IMEP injection strategy, $N_e = 1500$ rpm, VGT = 33%): effect on cylinder pressure.

In practical applications, the masses considered (fresh air and burned gas) cannot be measured. However, equivalent variables can be considered. Controlling these two masses is equivalent to controlling the intake pressure $P_{int}$ (corresponding to $M_{asp,air} + M_{asp,bg}$) and the burned gas rate $F_{int}$ (representing the ratio $M_{asp,bg}/(M_{asp,air} + M_{asp,bg})$).

In this context, the control problem addressed is a fast transition problem for a two-state, two-output, two-input system. The states are $P_{int}$ and $F_{int}$. The control inputs are the variable-geometry turbocharger (VGT) actuator position $S_{vgt}(v_1)$ (ranging from 0 to 1) and the normalized effective area of the EGR valve $S_{egr}(v_2)$ (ranging from 0 to 1). Other extraneous inputs include the fueling rate $M_{fuel}$ and the engine speed $N_e$. These are not controlled but are measured.

### 1.3. Control strategy

In terms of a control strategy, most studies consider the following setup: both the intake pressure and the intake

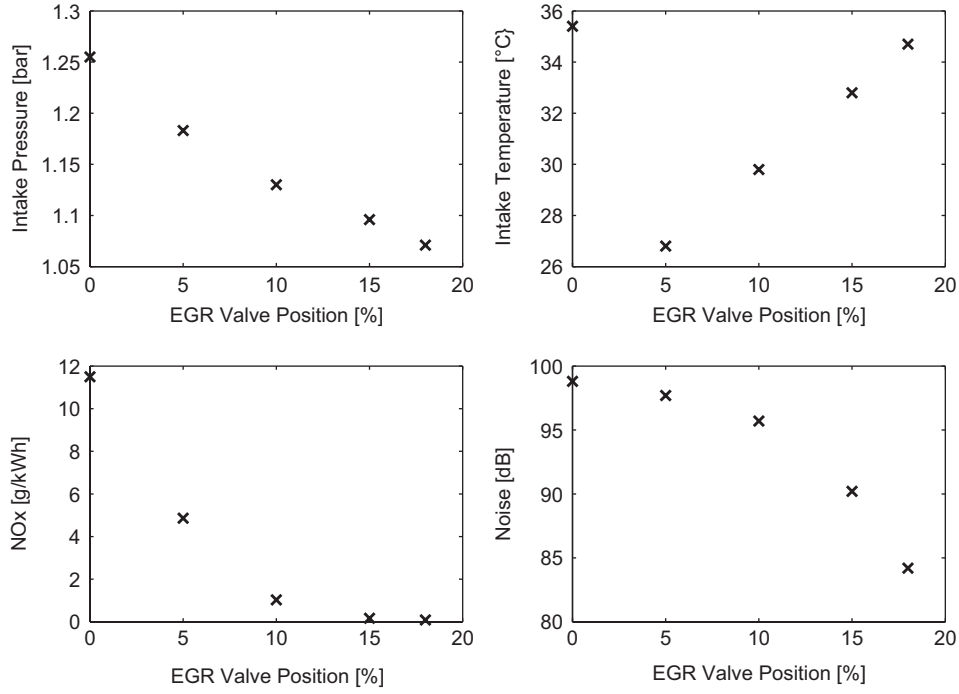


Fig. 2. Experimental variation of the EGR valve under the fixed operating conditions described for Fig. 1: effect on the intake pressure, intake temperature, $NO_x$ and noise.

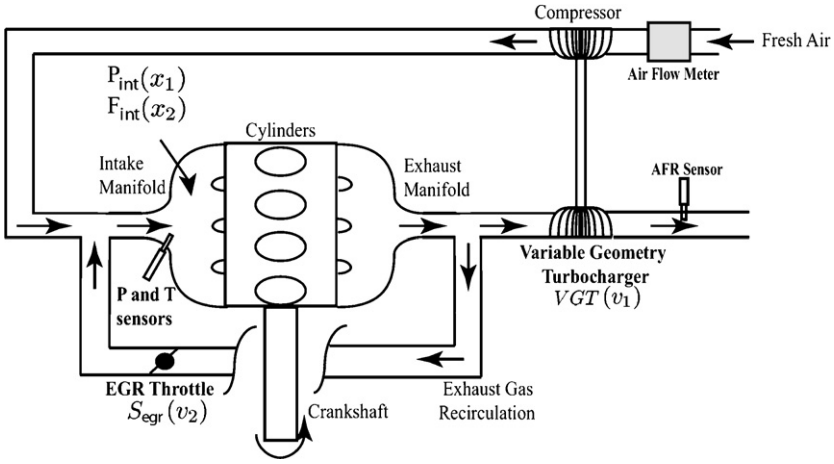


Fig. 3. Airpath system. The sensors used in the control setup are shown in gray (air flowmeter, AFR sensor, and intake pressure and temperature sensor). The inputs are the variable-geometry turbocharger (VGT) ($v_1$) and the EGR valve ($v_2$). The state variables are the intake pressure $P_{int}$ ($x_1$) and the burned gas ratio (BGR) $F_{int}$ ($x_2$).

Table 1
Nomenclature

| Symbol | Quantity | Unit | Variable |
|---|---|---|---|
| $P_{int}$ | Pressure in the intake manifold | Pa | $x_1$ |
| $F_{int}$ | Burned gas fraction in the intake manifold | – | $x_2$ |
| $\Theta_{egr}$ | EGR flow when the EGR valve is fully open | $kg\,s^{-1}$ | $x_3$ |
| $D_{air}$ | Manifold air flow | $kg\,s^{-1}$ | $u_1$ |
| $D_{egr}$ | EGR flow | $kg\,s^{-1}$ | $u_2$ |
| $S_{vgt}$ | Normalized variable-geometry turbocharger position | – | $v_1$ |
| $S_{egr}$ | Normalized effective area of the EGR valve | – | $v_2$ |
| $D_{asp}$ | Flow aspirated into the cylinders | $kg\,s^{-1}$ | |
| $F_{egr}$ | Burned gas fraction in the EGR pipe | – | |
| $F_{exh}$ | Burned gas fraction in the exhaust manifold | – | |
| $M_{asp,air}$ | Air mass aspirated in the cylinder | kg | |
| $M_{asp,bg}$ | Burned gas mass aspirated in the cylinder | kg | |
| $M_{int}$ | Total mass in the intake manifold | kg | |
| $M_{int,bg}$ | Burned gas mass in the intake manifold | kg | |
| $N_e$ | Engine speed | rpm | |
| $R$ | Ideal gas constant | $J\,kg^{-1}\,K^{-1}$ | |
| $T_{int}$ | Temperature in the intake manifold | K | |
| $V_{cyl}$ | Cylinder volume | L | |
| $V_{int}$ | Intake manifold volume | L | |
| $\eta_{vol}$ | Volumetric efficiency | – | |
| $\gamma$ | Specific heat ratio (fresh air) | – | |

airflow are closely controlled using an EGR throttle ($v_2$ in Fig. 3) and a VGT ($v_1$ in Fig. 3) using gain scheduling PI controllers (Stefanopoulou, Kolmanovsky, & Freudenberg, 2000; van Nieuwstadt et al., 1998; van Nieuwstadt, Kolmanovsky, Moraal, Stefanopoulou, & Janković, 2000). The PI gains are calibrated with respect to the engine speed and fueling rate. Jung and Glover (2003, 2005) used a linear parameter-varying (LPV) formulation with a $H_\infty$ loop-shaping control strategy to regulate the intake pressure and airflow. In these cases, no air fuel ratio (AFR) sensor was used so that the same instrumentation as for classical commercial diesel engines could be adopted. Controlling both the intake and exhaust pressures has been reported by Ammann, Fekete, Guzzella, and Glattfelder (2003). Janković and Kolmanovsky (1998, 2000) used a constructive Lyapunov technique to control the AFR and the EGR fraction to set points that were determined by the operating conditions during quasi-steady-state operation. For that purpose, the intake pressure, the intake mass airflow and the exhaust pressure were used, along with several changes in coordinates.

Intake pressure and temperature sensors and an air mass flow sensor (as in commercial diesel engines) are also used. Nevertheless, in the presented study, no exhaust pressure sensor was used for cost and reliability reasons. Instead, an AFR sensor was used in the exhaust manifold to obtain a precise insight into the gas composition.

Previous studies have proved both the relevance of and the need for multivariable control strategies. In this context, a simple but innovative solution is presented. A motion planning strategy is proposed in which a feedforward term is complemented by a tracking controller. The driver torque demand is first translated into in-cylinder mass set points, and then into a motion planning problem involving the burned gas ratio (BGR) and the intake manifold pressure. An explicit unconstrained transition is computed. The use of well-chosen tuning parameters should ensure that this transition is consistent with physically important constraints on the inputs. If not, the open-loop histories are automatically saturated and eventually provide convergence in any case.

In this paper, two components of the proposed control strategy are described in detail:

(i) *A feedforward motion-planning open-loop controller that uses the intake airflow $D_{air}$ and the EGR flow $D_{egr}$ as*

*inputs*: This is based on explicit inversion of the airpath dynamics. Although the flows are not real actuators, they represent a relevant equivalent set of inputs for two reasons: the flows appear very simply in balance equations, and all the constraints that are required to run the engine are easily written in terms of flows. Constraints are explicitly taken into account in this feedforward control derivation stage.

(ii) *An observer/controller to track the open-loop trajectory*: An observer to estimate the composition in the intake manifold and the EGR flow is also used. This is a Luenberger-style observer that reconstructs poorly known input variables from the intake pressure measurements. This observer is used for a single reason. It is required to guarantee (as far as estimation can actually guarantee) that the actual EGR flow equals its planned value. This is achieved using a SISO closed-loop controller (PI) acting on the normalized effective area of the EGR valve. The actual intake airflow is also controlled to track its planned value using a PI controller. This controller acts on the normalized VGT position.

Extensive experimental results, including partial ECE cycle tests, are reported. The results of the study demonstrate that motion planning is an effective solution for controlling airpath dynamics.

The remainder of the paper is organized as follows. In Section 2, the control problem is identified and the intake manifold model used for the study is described. Section 3 contains a description of the proposed control strategy. In Section 3.2, the fully actuated airpath dynamics is decoupled according to a simple motion-planning strategy in which physical input constraints are explicitly identified. In addition, a tuning methodology is provided. In Section 3.3, the design of the observer required for real implementation is described. Experimental results are reported for a four-cylinder HCCI engine in Section 4. Conclusions and future directions are provided in Section 5.

## 2. Control problem and system modeling

### 2.1. Intake manifold modeling

Numerous reports in the literature (Kao & Moskwa, 1995; Tsai & Goyal, 1986) present mean-value engine modeling as a reliable and efficient way to represent engine dynamics. These studies used temporal and spatial average values of the relevant temperatures, pressures and mass flow rates to generate a seven-state reference model. The seven states are the intake and exhaust manifold pressures, temperatures, and compositions, and the turbocharger speed. Because the model complexity affects the control design, most researchers usually consider a preliminary model of three states (Janković & Kolmanovsky, 2000; Jung & Glover, 2005; Stefanopoulou et al., 2000; van Nieuwstadt et al., 1998). In this context, a further reduction to two states is proposed. The motivation for this simplification is provided in the following subsection.

#### 2.1.1. Modeling assumptions

First, the standard assumption that temperature fluctuations in the intake manifold can be neglected (Hendricks et al., 1996) is adopted. Of the seven usual state variables, two are eliminated. The above-mentioned model reduction (Janković & Kolmanovsky, 2000; Jung & Glover, 2005; Stefanopoulou et al., 2000; van Nieuwstadt et al., 1998) yields a three-dimensional reference control model using the intake pressure, the exhaust pressure and the turbocharger speed as states. Composition dynamics are not taken into account because the corresponding two states (intake and exhaust composition) are difficult to measure and are only weakly observable from the remaining three states. In the present case, an AFR sensor located downstream of the turbine was used to represent the composition in the exhaust manifold. This major difference from typical setups prompted us to substitute the exhaust pressure dynamics with the composition dynamics. Finally, the turbocharger was considered to be in a steady state at all times. The reason for this simplification is that the turbocharger speed dynamics is very slow compared to the pressure and composition dynamics. In the present study, the turbocharger speed was modeled as a static function of the intake pressure $P_{int}$ and the intake airflow $D_{air}$. This reduces the problem to a two-dimensional state (the intake pressure, $P_{int}$, and composition $F_{int}$).

#### 2.1.2. State space model

Two balance equations provide the following model.

(i) *Total mass balance in the intake manifold*: The ideal gas law for the intake manifold leads to $P_{int}V_{int} = M_{int}RT_{int}$. Assuming that variations in temperature are small, the mass balance can be written as

$$\dot{P}_{int} = \frac{RT_{int}}{V_{int}}(D_{air} + D_{egr} - D_{asp}). \quad (1)$$

Classically (Heywood, 1988), the aspirated flow is modeled under the form $D_{asp} \triangleq \eta_{vol}(P_{int}, N_e)(P_{int}/RT_{int})V_{cyl}N_e/120$, where $V_{cyl}$ is the cylinder volume, $\eta_{vol}$ is the volumetric efficiency, which is experimentally determined, and $\eta_{vol}(P_{int}, N_e)$ is eventually defined using a look-up table.[2]

(ii) *Composition balance in the intake manifold*: The BGR $F_{int}$ is the fraction of burned gas in the intake manifold and can be expressed as $F_{int} \triangleq M_{int,bg}/M_{int}$. The composition of the EGR ($F_{egr}$) is the composition in the exhaust manifold ($F_{exh}$) delayed by transport

[2]The volumetric efficiency also depends on the exhaust pressure. Nevertheless, the dependence in the steady state can mainly be attributed to the intake manifold pressure. Therefore, only the intake pressure and the engine speed in the volumetric efficiency model are considered.

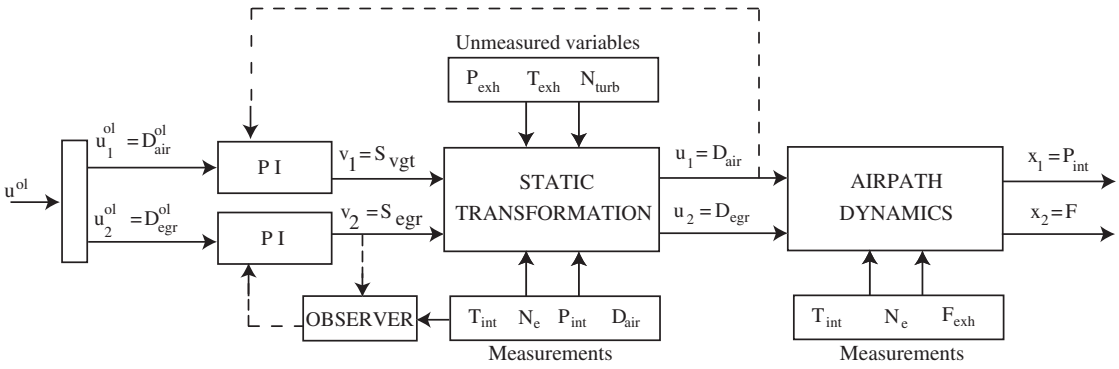


Fig. 4. Input/output scheme of the airpath dynamics. The actual control variables are $(v_1, v_2)$, and $u_1$ and $u_2$ are the variables directly appearing in the balance equations.

through the EGR pipe. This delay is considered as negligible, i.e. $F_{egr} = F_{exh}$, because a high-pressure EGR loop is considered. The mixing dynamics is modeled as

$$\dot{F}_{int} = \frac{RT_{int}}{P_{int}V_{int}}(D_{egr}(F_{exh} - F_{int}) - D_{air}F_{int}). \tag{2}$$

Eqs. (1) and (2) can be formally rewritten.

$$x_1 = P_{int}, \quad u_1 = D_{air}, \quad \alpha_{int} \triangleq \frac{RT_{int}}{V_{int}},$$

$$x_2 = F_{int}, \quad u_2 = D_{egr}, \quad \beta_{int} \triangleq \frac{1}{RT_{int}} V_{cyl} \frac{N_e}{120}.$$

The reference dynamics for the airpath is

$$\begin{cases} \dot{x}_1 = \alpha_{int}(u_1 + u_2 - \beta_{int}\eta_{vol}(x_1, N_e)x_1), \\ \dot{x}_2 = \dfrac{\alpha_{int}}{x_1}(F_{exh}u_2 - (u_1 + u_2)x_2). \end{cases} \tag{3}$$

This is represented as the input/output system depicted in Fig. 4 (right).

### 2.1.3. Mathematical assumptions

Since both $T_{int}$ and $N_e$ are strictly positive and upper-bounded (which is experimentally true), one can equivalently state that there must exist a set of constant parameters $(\alpha_m, \alpha_M, \beta_m, \beta_M)$ such that $0 < \alpha_m \leqslant \alpha_{int} \leqslant \alpha_M$ and $0 < \beta_m \leqslant \beta_{int} \leqslant \beta_M$. On the other hand, it is assumed that the aspirated flow $D_{asp}$ uniformly increases with the intake pressure $x_1$. Let us define $h_{Ne}(x_1) \triangleq \eta_{vol}(x_1, N_e)x_1$. Suppose that there exists a constant $\underline{h}$ such that, for all $x_1 > 0$, $(\partial h_{Ne}/\partial x_1)(x_1) \geqslant \underline{h} > 0$. Experimentally, this assumption is easy to validate. This allows us to define $x_{1,m} \triangleq h_{Ne}^{-1}(u_{min}/\beta_M) > 0$ and $x_{1,M} \triangleq h_{Ne}^{-1}(u_{max}/\beta_m) > x_{1,m}$.

## 2.2. Input constraints

In model (3), input constraints need to be accounted for. These are twofold.

(i) *Constraints on flow variables*: By definition of the input flows, the input signals $u_1$ and $u_2$ need to be positive. In addition, to take into account the physical limitations of the engine, the total input flow must be strictly positive and upper-bounded. To summarize, there must exist two constants $u_{min}$ and $u_{max}$ such that $0 < u_{min} \leqslant u_1 + u_2 \leqslant u_{max}$.

(ii) *Sufficient conditions for misfire avoidance*: A necessary condition to successfully pass normalized tests (such as the ECE cycle) is to avoid misfires and the implied peaks in pollutant emissions. Such misfires are more likely to occur at high EGR rates. A simple strategy can address this issue. Conservatively, misfire avoidance is guaranteed provided the following input constraints are satisfied: $C(u) \triangleq F_{exh}u_2/(u_2 + u_1) \leqslant \overline{C} < 1$.

Combining these constraints, the set of feasible inputs $\mathscr{U}$ is defined as

$$\mathscr{U} \triangleq \left\{ (u_1, u_2) / u_1 > 0, u_2 \geqslant 0, u_{min} \leqslant u_1 + u_2 \leqslant u_{max} \text{ and } F_{exh}\frac{u_2}{u_2 + u_1} \leqslant \bar{C} \right\}. \tag{4}$$

Its boundary is noted $\partial\mathscr{U}$.

## 2.3. Control problem

The objective is to steer system (3) from a given state $x = \underline{x}$ to another state $x = \bar{x}$. During this transition, the input variables must remain in $\mathscr{U}$.

# 3. System properties and control strategy

## 3.1. System properties

System (3) has some interesting properties. First, it is fully actuated. Thus, it is linearizable by non-linear static feedback: $(x_1, x_2)$ are the linearizing outputs. The motion-planning problem is readily solved by imposing the $(x_1, x_2)$ histories and computing the corresponding inputs (Chauvin, Corde, Petit, & Rouchon, 2006). Second, it is stable. This property is used in the motion-planning strategy. The two following propositions have been proved in Chauvin, Corde, and Petit (2006) and Chauvin (2006).

**Proposition 1.** *Let* $\mathscr{X} \triangleq [x_{1,m}, x_{1,M}] \times [0, \bar{C}]$ *be a non-empty subset of* $\mathbb{R}^2$. *For any initial condition* $x(0) = (x_1(0), x_2(0)) \in \mathscr{X}$, *and for any control input* $u$ *such that* $u(t) \in \mathscr{U}$ *defined in* (4) *for all* $t \geqslant 0$, *the solution* $x(t)$ *of* (3) *remains in* $\mathscr{X}$ *for all* $t \geqslant 0$. *The* (*functions*) *vector* $(x, u)$ *is said to be a* feasible trajectory.

**Proposition 2.** *Consider a* feasible reference trajectory $(x^r, u^r)$. *Feed* (3) *with the control input* $u^r$. *Then the error state* $x - x^r$ *globally exponentially converges to* 0.

The latter proposition is the key to understanding the proposed approach. Provided the control values chosen are feasible (i.e. belong to $\mathscr{U}$), it is sufficient to use them as inputs in the airpath system to exponentially reach a desired reference trajectory. From this point of view, the airpath control problem appears to be easily tractable by technique based on motion planning. For implementation, this strategy only needs to be complemented by an estimation technique to recover variables that are not measured and are required in the open-loop control derivation.

### 3.2. Airpath feedforward control

To generate feasible transition input histories, the control strategy uses a sequence of four subprocedures: (i) set-point computations using static maps; (ii) trajectory generation; (iii) model inversion; and (iv) saturation of the open-loop control values. Feedforward control laws are computed for (3) as follows.

(i) *Set-point computation: from the driver torque request* $\mapsto x^{sp}$: The driver request considered here is the accelerator position. First, taking into account the gearbox configuration, this request is translated into a torque control objective under the form of an indicated mean effective pressure (IMEP) setpoint. The setpoints (denoted as $x^{sp}$) for the intake pressure and the BGR are then inversely given by experimentally calibrated static maps for the $(\mathrm{IMEP}^{sp}, N_e)$ operating range. The engine speed $N_e$ is not modeled, but is directly measured.

(ii) *Motion planning*: $x^{sp} \mapsto x^{mp}$: Because $\mathrm{IMEP}^{sp}$ is arbitrarily specified by the driver, $t \mapsto x_1^{sp}(t)$ and $t \mapsto x_2^{sp}(t)$ may not be smooth or monotonous. These signals must be filtered to correspond to feasible trajectories of (3). This can be achieved using many different methods. Here, the proposed approach, besides other interesting properties (Chauvin, Corde & Petit, 2006; including ease of handling through convergence analysis), is easy to tune. To move from a current steady state $\underline{x}$ to a target state $\overline{x}$, interpolation formula (6) is used. In terms of coordinates, this defines $x_1^{\mathrm{mp}}$ and $x_2^{\mathrm{mp}}$. Let

$$\phi(t, T) = \begin{cases} 0 & \text{for } 0 \geqslant t, \\ \left(\dfrac{t}{T}\right)^2 \left(3 - 2\dfrac{t}{T}\right) & \text{for } 0 \leqslant t \leqslant T, \\ 1 & \text{for } T \leqslant t, \end{cases} \tag{5}$$

where $T$ is a positive constant. Note that $T_1$ and $T_2$ are two positive constants. The interpolation considered is

$$\begin{aligned} x_1^{\mathrm{mp}}(t) &= \underline{x}_1 + (\overline{x}_1 - \underline{x}_1)\phi(t, T_1) \quad \text{and} \\ x_2^{\mathrm{mp}}(t) &= \underline{x}_2 + (\overline{x}_2 - \underline{x}_2)\phi(t, T_2). \end{aligned} \tag{6}$$

(iii) *Model inversion*: $x^{mp} \mapsto u^{mp}$: Following Fliess, Lévine, Martin, and Rouchon (1995), an analytical expression for the input can be derived from the state variables and their first-derivative histories. In fact,

$$\begin{cases} u_1 + u_2 = \eta_{vol}(x_1, N_e)\beta_{int} x_1 + \dfrac{1}{\alpha_{int}}\dot{x}_1 \\ -x_2 u_1 + (F_{exh} - x_2)u_2 = \dfrac{1}{\alpha_{int}}\dot{x}_2 x_1. \end{cases} \tag{7}$$

This can be rewritten as

$$u_1 = f_1(x, \dot{x}) \quad \text{and} \quad u_2 = f_2(x, \dot{x}), \tag{8}$$

with

$$\begin{cases} f_1(x, \dot{x}) = \dfrac{1}{F_{exh}}\left(\dfrac{F_{exh} - x_2}{\alpha_{int}}\dot{x}_1 - \dfrac{1}{\alpha_{int}}\dot{x}_2 x_1 \right. \\ \qquad \left. + (F_{exh} - x_2)\eta_{vol}(x_1, N_e)\beta_{int} x_1\right), \\ f_2(x, \dot{x}) = \dfrac{1}{F_{exh}}\left(\dfrac{1}{\alpha_{int}} x_2 \dot{x}_1 + \eta_{vol}(x_1, N_e)\beta_{int} x_2 x_1 \right. \\ \qquad \left. + \dfrac{1}{\alpha_{int}}\dot{x}_2 x_1\right). \end{cases} \tag{9}$$

In the last expressions, $F_{exh}$, $\alpha_{int}$, $N_e$, and $\beta_{int}$ are all available from sensor measurements. The open-loop control law $(u_1^{\mathrm{mp}}, u_2^{\mathrm{mp}})$ corresponding to any desired $(x_1^{\mathrm{mp}}, x_2^{\mathrm{mp}})$ trajectory (defined by formula (6)) is uniquely defined by

$$\begin{aligned} u_1^{\mathrm{mp}} &= f_1(x_1^{\mathrm{mp}}, \dot{x}_1^{\mathrm{mp}}, x_2^{\mathrm{mp}}, \dot{x}_2^{\mathrm{mp}}) \quad \text{and} \\ u_2^{\mathrm{mp}} &= f_2(x_1^{\mathrm{mp}}, \dot{x}_1^{\mathrm{mp}}, x_2^{\mathrm{mp}}, \dot{x}_2^{\mathrm{mp}}). \end{aligned} \tag{10}$$

(iv) *Input constraints*: $u^{mp} \mapsto u^{ol}$: To take the input constraints into account, feasible control is defined as

$$u^{\mathrm{ol}}(t) \triangleq \arg\left(\min_{u \in \mathscr{U}} (u_1 - u_1^{\mathrm{mp}}(t))^2 + (u_2 - u_2^{\mathrm{mp}}(t))^2\right), \tag{11}$$

where $u_1^{\mathrm{mp}}(t)$ and $u_2^{\mathrm{mp}}(t)$ are defined by (10). For all $t \geqslant 0$, $u^{\mathrm{ol}}(t)$ is the projection of $u^{\mathrm{mp}}(t) = (u_1^{\mathrm{mp}}, u_2^{\mathrm{mp}})(t)$ onto the set $\mathscr{U}$. In the optimization problem defined by (11), both the objective function and the admissible set $\mathscr{U}$ are convex. Thus, a uniquely defined solution $x^{\mathrm{ol}}$ always exist. In fact, this solution can be analytically computed in a straightforward way by enumerating the nine possible solutions.

#### 3.2.1. Tuning of constrained motion planning

The open-loop trajectories (6) are tuned by two parameters: $T_1$ and $T_2$. Certainly, this is a rather approximate description of possible approaches. Further

developments could include definition of the interpolation function $\phi$ by B-spline functions (Milam, 2003). Motivation of this restrictive choice is again the requirements of the real-time control system running at 100 Hz at 1500 rpm and the *relatively* heavy computational burden involved in other approaches.

In fact, one can compute *analytically* $T_1$ and $T_2$ to obtain feasible inputs. First, by taking $T_1 = T_2 = +\infty$, feasible input histories are obtained because $\mathscr{U}$ is convex. Then, by taking small enough $T_1 = T_2 = \varepsilon$, such that the transition is accelerated, the input histories eventually leave the set $\mathscr{U}$ because the derivative terms go to $+\infty$. Finally, $T_{M,1}$ and $T_{M,2}$ are analytically computed such that the control values meet the constraints defined in (12) (Chauvin, Corde & Petit 2006).

The following proposition is important because it provides a rule-of-thumb type of tuning method.

**Proposition 3.** *Consider the motion-planning strategy* (6)–(10) *aimed at steering the system from steady state* $(\underline{x},\underline{u})$ *to* $(\overline{x},\overline{u})$. *If* $(\underline{u},\bar{u}) \in (\mathscr{U}\backslash\partial\mathscr{U})^2$, *then by choosing large enough* $T_1 > T_{M,1}(\varepsilon)$ *and* $T_2 > T_{M,2}(T_{M,1}(\varepsilon),\varepsilon)$ *(with* $\varepsilon \triangleq \min\{dist(\underline{u},\partial\mathscr{U}), dist(\bar{u},\partial\mathscr{U})\}$*) as defined in* (12), $u^{mp}(t) \in \mathscr{U}\backslash\partial\mathscr{U}$ *for all* $t>0$.

The lower-bounding functions are

$$T_{M,1}(\varepsilon) \triangleq \frac{2}{\varepsilon}\frac{|\overline{x}_1 - \underline{x}_1|}{\alpha_{int}} \quad \text{and} \quad T_{M,2}(T_1,\varepsilon) \triangleq \frac{2}{\varepsilon}\frac{|\overline{x}_2 - \underline{x}_2|}{\alpha_{int}\beta_{int}\,\underline{\eta_{vol}} - 3|\overline{x}_1 - \underline{x}_1|/2T_1\min\{\overline{x}_1,\underline{x}_1\}}. \tag{12}$$

Furthermore, if $\bar{u} \in \partial\mathscr{U}$, it can be shown that there exist $T_1>0$ and $T_2>0$ such that the constraints are violated by less than any prescribed $\varepsilon$. In other words, the distance $\mathrm{dist}(u^{\mathrm{mp}}(t),\mathscr{U})$ is below $\varepsilon$ for all $t \geqslant 0$. From this property, the calibration strategy uses $T_1 = T_{M,1}(\varepsilon)$ and $T_2 = T_{M,2}(T_1,\varepsilon)$.

### 3.3. Airpath observer

As shown in Fig. 4, the real control variables are not $(u_1,u_2)$, but rather $(v_1,v_2)$. Equivalently, one can use $(v_1,v_2)$, which uniquely define $(u_1,u_2)$, provided several variables are known. Some of the required variables are measured ($T_{int}$, $N_e$, $P_{int}$, $u_1 = D_{air}$), whereas some are not ($P_{exh}$, $T_{exh}$, $N_{turb}$). The latter variables are typically not used for control purposes in commercial cars owing to cost issues or a lack of accuracy. In the following, how to recover these variables that are not measured is explained. This is necessary to compute $\hat{u}_2$, an estimated value of the EGR flow that is used to control $u_2$ through the closed-loop controller (on the other hand, the airflow $u_1$ is directly measured). As described by Heywood (1988), a common model is $u_2 \triangleq v_2\phi(P_{exh},T_{exh},P_{int})$, where $\phi$ is a non-linear function. Note that $\Theta_{egr} \triangleq \phi(P_{exh},T_{exh},P_{int})$, which represents the EGR flow if the EGR valve is open ($v_2 = 1$). This unknown variable needs to be reconstructed to evaluate the EGR flow $u_2$. For this purpose, a reference model dynamics is presented and an observer designed. This observer uses the output injection technique (Krener & Isidori, 1983; Krener & Respondek, 1985). The observer design follows from Chauvin, Corde, Petit and Rouchon (2006). Exponential convergence of the observer can be proven using Lyapunov arguments.

#### 3.3.1. Reference model

Let $x = [P_{int}\ \ F_{int}\ \ \Theta_{egr}]^{\mathrm{T}}$ be the state and $y = P_{int}$ be the measurement. Using (1) and (2), the reference dynamics can be written as

$$\begin{cases} \dot{x}_1 = \alpha_{int}(u_1 + v_2x_3 - \eta_{vol,map}(x_1,N_e)\beta_{int}x_1), \\ \dot{x}_2 = \dfrac{\alpha_{int}}{x_1}(F_{exh}v_2x_3 - (u_1 + v_2x_3)x_2), \quad y = x_1, \\ \dot{x}_3 = 0. \end{cases} \tag{13}$$

#### 3.3.2. Observer design

The proposed observer uses the following dynamical equation:

$$\begin{cases} \dot{\hat{x}}_1 = \alpha_{int}(u_1 + v_2\hat{x}_3 - \eta_{vol,map}(y,N_e)\beta_{int}\hat{x}_1) \\ \qquad -\alpha_{int}(l_1 - \eta_{vol,map}(y,N_e))\beta_{int}(\hat{x}_1 - y), \\ \dot{\hat{x}}_2 = \dfrac{\alpha_{int}}{y}(F_{exh}v_2\hat{x}_3 - (u_1 + v_2\hat{x}_3)\hat{x}_2), \\ \dot{\hat{x}}_3 = -l_3\alpha_{int}v_2(\hat{x}_1 - y), \end{cases} \tag{14}$$

with $(l_1,l_3)$ strictly positive constants (and $l_1>1$). It is evident that (14) is similar to (13) with additional tracking terms and inclusion of output measurement $y$. The unknowns are partially substituted with output measurements. The convergence of this observer was previously proved (Chauvin, Corde, Vigild, Petit, & Rouchon, 2006; Chauvin, 2006), leading to the following proposition.

**Proposition 4.** *When the EGR valve is open, i.e.* $v_2>0$, *the state of observer* (14) *exponentially converges to the state of system* (13).

This observer allows real-time converging estimation $\hat{u}_2 = v_2\hat{\Theta}_{egr}$ of the EGR flow $u_2$.

### 3.4. Airpath low-level controllers

The feedback control strategy aims to control $(v_1,v_2)$ in order to drive $(u_1,u_2)$ to $(u_1^{ol},u_2^{ol})$. For this purpose, fast PID controllers are added to the structure to provide further accuracy and robustness.

#### 3.4.1. $v_2$ to drive $\hat{u}_2$ to $u_2^{ol}$

Increasing $v_2$ corresponds to opening the EGR valve and thus increasing the EGR flow $u_2$. The flow response is almost instantaneous. Thus, a PI controller between the setpoint ($u_2^{ol}$) and the estimated ($\hat{u}_2$) with an anti-wind-up action on the normalized EGR flow is used on $v_2$. More precisely, $v_2 = u_2^{ol}/\hat{\Theta}_{egr} - k_{2,i}\int(u_2^{ol} - \hat{u}_2/\hat{\Theta}_{egr})\,\mathrm{d}t$.

#### 3.4.2. $v_1$ to drive $u_1$ to $u_1^{ol}$

Increasing the VGT position $v_1$, i.e. opening the guide vanes, leads to greater restriction of the exhaust gas flow and thus to a decrease in the exhaust manifold pressure. When the EGR valve $v_2$ is wide open (at low speed and low load, for example), an increase in $v_1$ results in a decrease in EGR flow $u_2$, which in turn increases the airflow $u_1$. When $v_2$ is almost closed, most of the exhaust gas must pass through the turbine. An increase in $v_1$ decreases the compressor power and thus increases the airflow. In this case, the VGT acts as a conventional wastegate, i.e. the VGT directly controls the turbocharger speed and the airflow $u_1$. Therefore, the steady-state gain from $v_1$ to $u_1$ strongly depends on the operating point. Thus, a gain-scheduled PID controller is designed to track the airflow setpoint $u_1^{ol}$. More precisely, $v_1 = -k_{1,p}(N_e, IMEP_{sp})(u_1^{ol} - u_1) - k_{1,i}(N_e, IMEP_{sp}) \int (u_1^{ol} - u_1)\,\mathrm{d}t$.

## 4. Experimental results

### 4.1. Implementation

The global control scheme is summarized in Fig. 5. The airpath observer block involves implementation of the observer described in Section 3.3. This block gives an estimation of the BGR and the EGR flow. The motion-planning block involves implementation of the motion-planning open-loop control strategy described in Section 3.2. Fast PID controllers are added to the structure to provide further accuracy and robustness. Their implementation is described in Section 3.4.

### 4.2. Two experimental representative transitions

Figs. 6 and 7 report experimental closed-loop results. The scenario is a varying torque demand at constant engine speed (1500 rpm) in both HCCI and conventional combustion modes.

#### 4.2.1. From $t = 102$ s to $t = 112$ s

Here, the transient under consideration is an IMEP transition at 1500 rpm in HCCI combustion mode. The

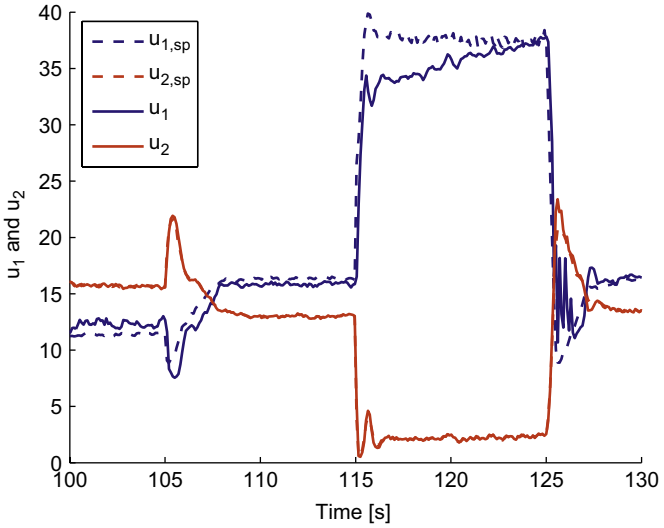


Fig. 6. Experimental results: IMEP transition from 2 to 5 bar, to 9 bar, to 5 bar, and then to 4 bar at 1500 rpm. Flow histories (dashed line, $u^{sp}$; solid line, $u$).

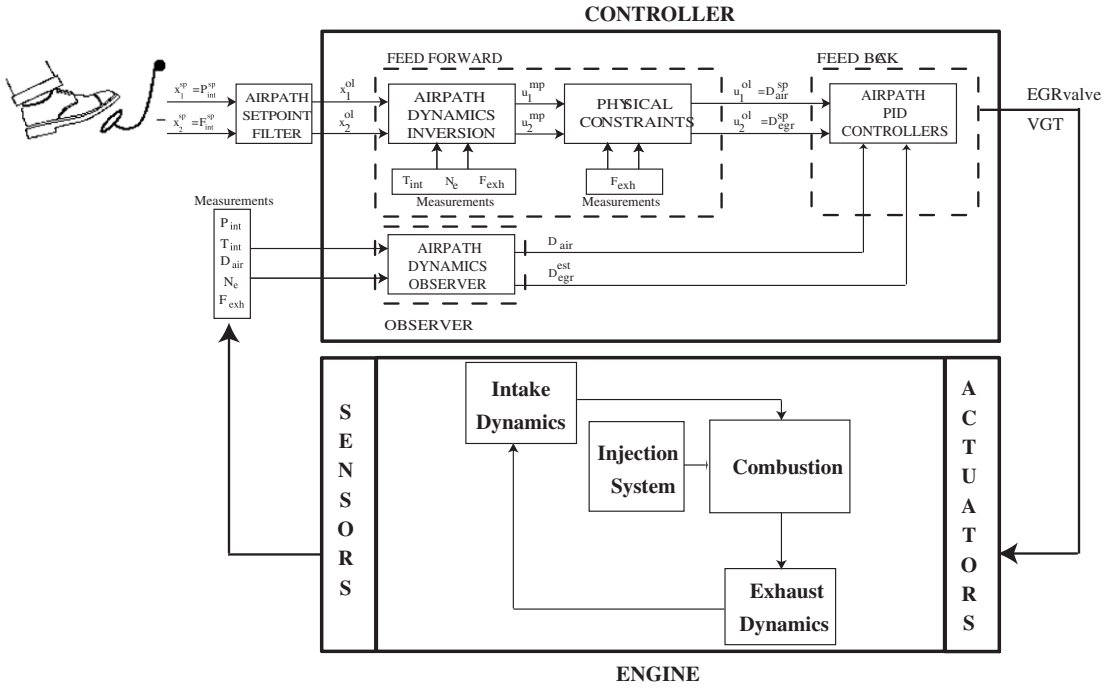


Fig. 5. Control scheme.

IMEP of the system starts at 2 bar and eventually reaches 5 bar. This transition aims at higher intake pressure and BGR setpoints. The starting and ending operating points are both in HCCI combustion mode. In contrast to all decentralized controllers, one can note that the controller takes into account the well-known non-minimum phase behavior of the system reported by (Kolmanovsky et al., 1997). More precisely, one can check that the main contribution to this is from the open-loop controller (the closed-loop control histories are very close to it). When the EGR valve opens, the flow increases, leading to a pressure rise in the intake manifold. Meanwhile, the exhaust pipe acts as a discharge for the VGT and opening of the pipe lowers the EGR supplied to the turbocharger, yielding a significant decrease in the exhaust manifold flow. The turbocharger slows down, which eventually causes a decrease in the intake manifold pressure. This phenomenon is delayed and slowed down by turbocharger inertia. Simple ramps and/or steps fail to allow the system to reach the desired setpoint. With the proposed control strategy, the model takes into account this complex behavior. The motion planning efficiently drives the system to its setpoint.

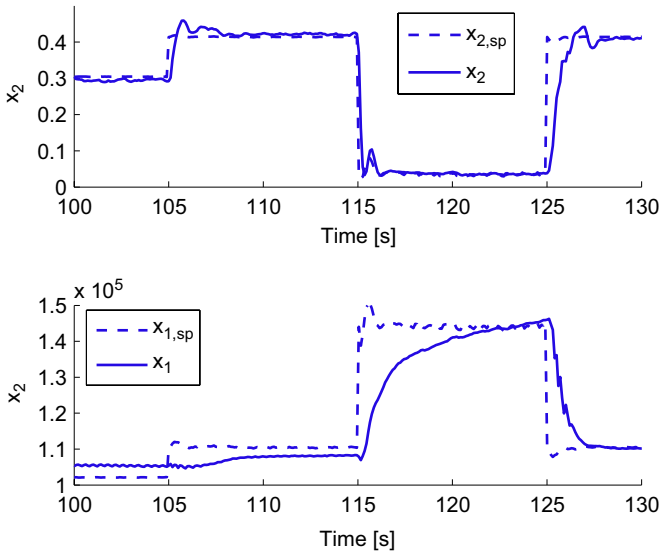


Fig. 7. Experimental results: IMEP transition described for 6. Top, intake pressure (dashed line, $x_1^{sp}$; solid line, $x_1$); bottom, BGR (dashed line, $x_2^{sp}$; solid line, $x_2$).

#### 4.2.2. *From $t = 112\,s$ to $t = 122\,s$*

In this case, the transient is a high increase in torque demand at 1500 rpm. Implicitly, the objective is to steer the system from a low load point with high EGR to a high load point with a significantly lower BGR. The proposed open-loop control strategy successively closes the EGR valve and closes the VGT with an overshoot. A resulting decrease in EGR flow and simultaneous increase in fresh air flow are evident. As expected for a motion-planning control strategy, this provides a soft landing for the state variables $x_1$ and $x_2$ onto their setpoints. During the transition, the open-loop control laws are indeed saturated. This results in a temporary mismatch between the airflow and its setpoint. This effect is particularly notable for this very large

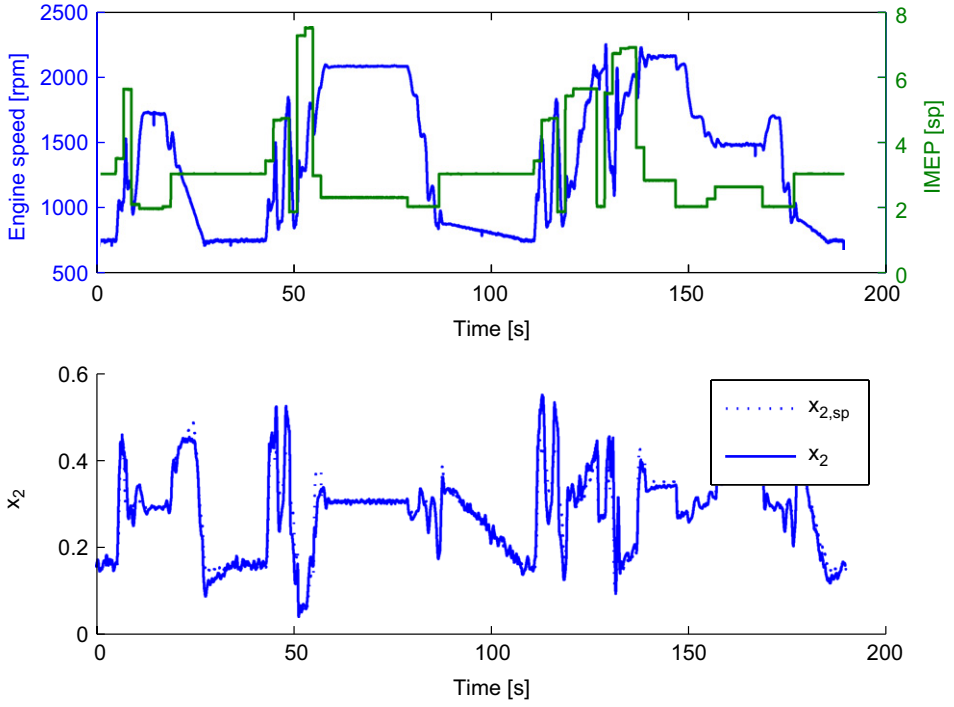


Fig. 8. Experimental results for the ECE cycle: top, engine speed/torque trajectory; bottom, BGR histories (dashed line, $x_2^{sp}$; solid line, $x_2$).

pressure transition, which was chosen for the sake of illustration.

Again, the transitions are smooth and present only small oscillations. It is interesting to note that, in the exact same setup, decentralized controllers fail to prevents both stalling and noise. The main reason for this seems to be the undesired BGR overshoot.

### 4.3. Experimental results for an ECE driving cycle

The control was tested on the ECE driving cycle, which is very difficult to handle with high EGR rates. Indeed, 85% of the cycle is performed in the HCCI combustion mode. The same calibration was maintained throughout the driving cycle. The engine speed/IMEP demand is presented in Fig. 8. The BGR is well tracked, as observed in Fig. 8. The dynamics is fast, and over- and undershoots are very limited and of short duration, which limits possible misfires and increased noise. As in the following cases, the EGR flow is almost perfectly tracked, and airflow tracking is good but slightly slow during large transitions. This is mostly due to turbocharger inertia. In summary, the results are good, even for a reasonably large transition, and the planned trajectory is well followed. High-pressure setpoints are more difficult to reach due to turbocharger inertia and friction. However, accurate tracking of the intake pressure is not required because, for pollutant reduction purposes, only the BGR needs to be closely controlled provided a limited AFR is guaranteed. Errors in the intake pressure will only lead to a very small error for torque production. Nevertheless, this problem will not arise in a vehicle because the engine speed and turbocharger speed increase in response to increases in torque production. This phenomenon is expected to be reduced in real-vehicle applications.

## 5. Conclusions and future work

The present study demonstrates the relevance of motion planning in the control of the (coupled) airpath dynamics of turbocharged diesel engines using EGR. For the HCCI combustion mode, very high BGR values need to be considered. Realistic test-bench cases prove that the proposed approach can handle such situations. Despite strong coupling and possible non-minimum phase dynamics, the airpath dynamics exhibits properties that make it easy to steer through the control strategy. Its triangular form yields exponential convergence over a wide range of setpoints. Moreover, input constraints can be added without jeopardizing the convergence. Compared to the static relationship $(IMEP^{sp}, N_e) \mapsto x^{sp}$, the motion-planning strategy can be considered, from a schematic point of view, as a dynamic mapping of the airpath.

Results from the present study were validated experimentally for a HCCI engine with a high-pressure EGR circuit and a variable-geometry turbocharger. The next step is to integrate the turbocharger dynamics to obtain more accurate control of the airflow. The control strategy will then be extended to other engine configurations, including a low-pressure EGR circuit, a waste gate, a two-stage turbocharger, and an intake throttle. The same control strategy can be applied. The main modification will be to decentralize the control in order to use all the actuators for control of the airflow $D_{air}$ and EGR flow $D_{egr}$.

## References


Ammann, M., Fekete, N., Guzzella, L., & Glattfelder, A. (2003). Model-based control of the VGT and EGR in a turbocharged common-rail diesel engine: Theory and passenger car implementation. In *Proceedings of the SAE conference*, Paper 2003-01-0357.

Chauvin, J. (2006). *Estimation and control of a diesel HCCI engine. Estimation for time periodic systems*. Ph.D. Thesis, École des Mines de Paris.

Chauvin, J., Corde, G., & Petit, N. (2006). Constrained motion planning for the airpath of a diesel HCCI engine. In *Proceedings of the conference on decision and control*.

Chauvin, J., Corde, G., Petit, N., & Rouchon, P. (2006). Experimental motion planning in airpath control for HCCI engine. In *Proceedings of the American control conference*.

Chauvin, J., Corde, G., Vigild, C., Petit, N., & Rouchon, P. (2006). Air path estimation on diesel HCCI engine. In *Proceedings of the SAE conference*, Paper 2006-01-1085.

Fliess, M., Lévine, J., Martin, Ph., & Rouchon, P. (1995). Flatness and defect of nonlinear systems: introductory theory and examples. *International Journal of Control*, *61*(6), 1327–1361.

Hendricks, E., Chevalier, A., Jensen, M., Sorenson, S., Trumpy, D., & Asik, J. (1996). Modelling of the intake manifold filling dynamics. In *Proceedings of the SAE conference*.

Heywood, J. (1988). *Internal combustion engine fundamentals*. New York: McGraw-Hill.

Janković, M., & Kolmanovsky, I. (1998). Robust nonlinear controller for turbocharged diesel engine. In *Proceedings of the American control conference*.

Janković, M., & Kolmanovsky, I. (2000). Constructive Lyapounov control design for turbocharged diesel engines. *IEEE Transactions on Control Systems Technology*, *8*, 288–299.

Jung, M., & Glover, K. (2003). Control-oriented linear parameter-varying modelling of a turbocharged Diesel engine. In *Proceedings of the conference on control applications*.

Jung, M., & Glover, K. (2005). Comparison of uncertainty parameterisations for H-infinity robust control of turbocharged diesel engines. *Control Engineering Practice*, *13*, 15–25.

Kao, M., & Moskwa, J. (1995). Turbocharged diesel engine modelling for nonlinear engine control and estimation. *ASME Journal of Dynamic Systems Measurements and Control*, *117*, 21–30.

Kolmanovsky, I., Stefanopoulou, A., Moraal, P., & van Nieuwstadt, M. (1997). Issues in modelling and control of intake flow in variable geometry turbocharged engines. In *Proceedings of the 18th IFIP conference on system modelling and optimization*.

Krener, A., & Isidori, A. (1983). Linearization by output injection and nonlinear observers. *Systems & Control Letters*, *3*, 47–52.

Krener, A., & Respondek, W. (1985). Nonlinear observers with linearizable error dynamics. *SIAM Journal of Control Optimization*, *23*, 197–216.

Milam, M. (2003). *Real-time optimal trajectory generation for constrained systems*. Ph.D. Thesis, California Institute of Technology.

van Nieuwstadt, M., Moraal, P., Kolmanovsky, I., Stefanopoulou, A., Wood, P., & Criddle, M. (1998). Decentralized and multivariable designs for EGR-VGT control of diesel engine. In *Proceedings of the IFAC symposium on advances in automotive control*.

van Nieuwstadt, M., Kolmanovsky, I., Moraal, P., Stefanopoulou, A., & Janković, M. (2000). Experimental comparison of EGR-VGT control schemes for a high speed diesel engine. *IEEE Transactions on Control System Magazine*, *20*, 63–79.

Stefanopoulou, A., Kolmanovsky, I., & Freudenberg, J. (2000). Control of variable geometry turbocharged diesel engines for reduced emissions. *Proceedings of the IEEE Control Systems Technology*, *8*, 733–745.

Tsai, S.-C., & Goyal, M. (1986). Dynamic turbocharged diesel engine model for control analysis and design. In *Proceedings of the SAE conference*.